

1 **A Comprehensive Investigation of Refinery Preheaters Foulant Samples Originated by**
2 **Heavy Crude Oil Fractions as Heating Fluids**

3
4
5 Elaheh Behranvand^a, Mohammad Reza Mozdianfard^{a,*}, Emilio Diaz-Bejarano^b, Francesco Coletti^c, Pawel
6 Orzlowski^b and Sandro Macchietto^{b,c}

7
8
9 ^a Chem. Eng. Dep., Eng. Faculty, University of Kashan, Kashan, IRAN

10 ^b Dept. of Chem. Eng., Imperial College London, London SW7 2AZ, UK

11 ^c Hexxcell Ltd., Innovation Hub, White City Campus, 80 Wood Lane, London W12 0BZ, UK

12
13
14
15 **Abstract**

16 A deep understanding of the mechanisms responsible for fouling from both crude oils and
17 their fractions is paramount to ensure efficient energy recovery in heat exchangers of crude
18 preheat trains. In this work, seven samples of fouling deposits, carefully collected from a
19 number of refinery heat exchangers processing vacuum gas oil (VGO) and vacuum bottom
20 (VB) streams in an atmospheric crude preheat train were investigated using a range of
21 characterization techniques with the aim of identifying the underlying mechanisms that led to
22 deposition. Characterization of the deposits included morphological and physical examination,
23 fractionating solubility test, Scanning Electron Microscopy-Energy Dispersive X-Ray,
24 Combustion Analysis and X-Ray Diffraction. In all samples examined, more than 75wt% of the
25 deposits were identified as inorganic, with about 50wt% being FeS. At 270-300 °C, FeO(OH) was
26 also identified to be deposited on the tube surfaces made in Cr steel alloy, where more fouling
27 and less corrosion were evident compared to carbon steel (CS). These observations were found
28 in agreement with recent laboratory studies aimed at identifying the role of temperature and

29 tube material in petroleum corrosion. Furthermore, sulphur crystals were found in several VGO
30 fouling samples. Based on the experimental results obtained, a mechanism was proposed to
31 explain the corrosion fouling phenomenon, considered to be the underlying mechanism
32 affecting the refinery. The mechanism involves naphthenic acid attack to the tubes' metal
33 surface, decomposition of iron naphthenate, disproportion of iron oxide and sulphidation
34 reactions. The results highlighted the importance of studying deposits formed under industrial
35 conditions, timescales and variation of the deposition process, evidenced by the deposit
36 characteristics, along extensive heat exchanger networks.

37 **Keywords:** Refinery Foulant Characterisation; Fouling Mechanism; Corrosion; Vacuum Gas Oil; Vacuum Bottom; Iron
38 Oxide.

39 **1. Introduction**

40 Atmospheric crude distillation is the first process unit in oil refineries. The performance of the
41 distillation columns where oil is fractionated into products affects significantly that of the entire crude oil
42 refining process. The most important factor influencing the column performance is the crude oil inlet
43 temperature, together with the flowrates and temperatures of the recycled fluids. A significant portion of
44 the thermal energy in product streams leaving the distillation column is recovered by a network of heat
45 exchangers, the pre-heat train, in which the inlet crude oil is heated up before entering the furnace. The
46 study of fouling in these exchangers has been the subject of intense interest from both academia and
47 industry and its impact on operations, energy costs and environmental emissions has been well
48 documented [1,2], however the underlying phenomena are still largely poorly understood.

49 Many fouling mechanisms have been identified to occur in crude pre-heat trains [3]. These include
50 scaling (salt precipitation), corrosion, precipitation (by cooling, blending or breaking of emulsions),
51 chemical reaction (thermal cracking, polymerisation of conjugated olefins, aromatic growth, oxidation,
52 etc.), and particulate deposition (such as entrained coke, asphaltenes, iron sulphides) which could act

53 individually or in combination with each other. Characterization of fouling deposits is an important first
54 step in understanding the underlying mechanisms. For instance, when 10-15 wt% or more inorganic
55 components are detected in a fouling sample, this could be a good indication that either scaling, corrosion
56 and particulate are the possible mechanisms responsible for deposition [4] [5].

57 Several efforts are found in the literature attempting to standardise the generation, collection and
58 analysis of crude oil samples. One such effort is the analytical industrial protocol patented by Brons et al.
59 in 2004 [4]. The protocol details characterisation methods for solids collected in refinery heat exchangers,
60 that can be used to identify the mechanism/s involved in their generation. The analysis prescribed included
61 methylene chloride or toluene extraction, Scanning Electron Microscopy-Energy Dispersive X-ray
62 (SEM-EDX), Thermogravimetric Analysis (TGA), Elemental Analysis (EA) and Optical Microscopy
63 (OM) arranged as a sequential diagram. In 2006, an industrial task force published recommended
64 guidelines aimed at facilitating direct comparison between non-proprietary fouling data [5]. Techniques
65 included were Fourier transform infrared spectroscopy (FTIR), X-ray fluorescence (XRF), X-ray
66 diffraction (XRD), X-ray photoelectron spectroscopy and Nuclear magnetic resonance (NMR). In 2009,
67 Venditti et al. [6] applied some of these techniques following solubility tests, size exclusion
68 chromatography and UV-fluorescence to characterize four foulants deposited in a refinery heat exchanger
69 by desalted crude oil, kerosene, vacuum gas oil and crude oil residue. In another work, Young et al. [7]
70 employed the same analysis on deposits generated in a laboratory batch stirred cell. These deposits were
71 then characterised and their thermal data were correlated with oil and deposits taken from various process
72 conditions by measuring deposit thickness along and around the probe using a laser and coherent light
73 scanning procedure. Recently, Joshi in [8], announced that the same simplified analysis proposed by
74 Brons et al. [4] is sufficient for quantification of only a few elements, required to distinguish between the
75 most common mechanisms of crude oil fouling. He also described the concept of setting a mass balance
76 between the measured weight percentages of the identified elements to verify the quality of the results or
77 to specify the necessity of more analysis to recognise the possible missing elements.

78 Analysis of deposits formed in lab-tests may help improve the fundamental understanding of the
79 processed involved in fouling deposit formation. However, the conditions leading to deposition in
80 industrial systems are very difficult to reproduce in lab-test, as a result of the complexity of crude oil
81 composition, the frequent variation of feedstock and the long times scales for significant fouling build-up
82 (months or years). Obtaining reliable outcomes requires appropriately collecting fouling samples from the
83 heat exchangers in a refinery, while considering systematically their fluid properties and operating
84 conditions. Foulant samples deposited by hydrocarbon fluids are complex materials containing both
85 organics and inorganics. Their low solubility makes them unsuitable for characterization by common
86 analytical techniques [6], and adequate protocols for sample preparation are required prior to the chemical
87 characterization.

88 Following an uninterrupted 8-year field study on fouling of crude oil preheaters at a refinery in Iran
89 processing the same feedstock [9][10], in this paper, several foulant samples deposited by vacuum gas oil
90 and vacuum bottoms as heating fluids of crude oil were investigated. This was done by recording their
91 general appearance, then carrying out a fractionating solubility test, SEM-EDX, XRD and
92 combustion/CHN analysis. First, sample description, preparation and analysis in the experimental work
93 are described, with results elucidated in three categories of morphology, physical and chemical
94 characteristics. The presence of FeS and FeO(OH) is then discussed, taking into account laboratory case
95 studies and the role of temperature and tube material. A novel corrosion/deposition mechanism is
96 proposed to explain the observed results. Finally, the presence of sulphur crystals in the maltenes fractions
97 of some vacuum gas oil (VGO) foulant samples is noted and suggested for further investigations.

98 **2. Experimental**

99 2.1. Samples

100 Foulant samples were collected during a major shutdown of a crude oil distillation unit following a 4-
101 year period of operation. The collection was performed following water circulation and steam purging,

102 after which the tube bundles were pulled out of their shells. Five samples were taken from foulant
 103 deposited by VGO and two from VB as heating fluids (see Table 1). The foulant originated by VGO
 104 presented greater volume compared to those of the other heating fluids, included that formed by VB.

105 In the refining process, VGO (of Specific Gravity SG=0.9137) leaves the middle of the vacuum
 106 distillation column at about 300°C. It is then cooled in the crude oil preheaters and air coolers and partly
 107 recycled back to the column, with the remainder sent to a hydrocracking unit for conversion into more
 108 valuable products. VB (SG=1.0115), the heaviest material in the distillation columns, is pumped out from
 109 the bottom of the vacuum column at about 360°C to the hot-end preheat exchangers.

110 Operational information of samples including the fluids from which foulants were originated, the
 111 exchangers name, tube material and maximum bulk temperature ranges (input-output) are listed in Table
 112 1. As for the notation used in describing the foulant samples, VG and VB indicate the corresponding fluid,
 113 while TO and TI indicate whether the sample was taken from tube outer or inner surface, respectively.
 114 The higher the number at the end of the sample names, the higher was the operating temperature for that
 115 fluid.

117 **Table 1- The operational information of foulant samples**

Samples	VGTO-1	VGTO-2	VGTO-3	VGTO-4	VGTO-5	VBTI-1	VBTO-2
Origin Fluid	VGO	VGO	VGO	VGO	VGO	VB	VB
Exchanger Name	E1A	E2B	E2A	E3B	E3A	E4	E5
Tube Material	C.S.	C.S.		1¼ Cr-1/2 Mo		C.S.	5Cr-1/2Mo
Max Bulk Temp Range (°C)	180-120	254-200		300-230		230-190	280-250

118

119 **2.2. Preparation**

120 The analysis preparation step consisted in removing the free bulk fluid trapped in the foulant contents
 121 and converting it into powder for further analysis in the available equipment. Sufficient quantity (in 10
 122 to1 ratio) of n-heptane was added to 10-25g of sample in an airtight jar and kept for at least 4h at room
 123 temperature. Using a vacuum pump, the mixture was filtered repeatedly using additional solvent until a

124 colourless filtrate was obtained. This way, it was safe enough to assume that all trapped fluid was removed.
125 The leftover on the filter paper was dried for at least 12h in an oven at 60-80°C, grinded with 60 mesh
126 (250µm) sieves, and mixed thoroughly [8] [11].

127 2.3. Analysis

128 With a view to maintaining a simple strategy to characterise foulant samples and explore the prevailing
129 mechanism/s, a set of analytical tests was carried out on the raw samples and powders prepared as
130 explained above.

131 The general appearance of the raw samples was first recorded using a digital camera. The sample layer
132 thickness was also measured when possible using a digital calliper with an accuracy of ± 0.01 mm.

133 A solvent extraction method, used elsewhere for product characterisation in hydrocracking studies [12]
134 [13], was employed to fractionate the raw samples into three groups: maltenes (heptane soluble),
135 asphaltenes (heptane insoluble, toluene soluble) and the remaining insoluble portion. To this purpose, a
136 0.2-0.5 g sample was placed in a jar (labelled as insoluble part) and mixed with 8.0 mL of heptane for 2h,
137 before centrifugation at 2000rpm for 20min. The supernatant was then separated and injected into the
138 maltenes jar, while heptane was added to the rest of the sample to repeat the procedure at least three times,
139 or until the supernatant became clear. Subsequently, toluene was added to the solids and mixed for 2h and
140 centrifuged, in order to extract the top phase which was transferred to the asphaltenes jar. Finally, three
141 jars containing heptane soluble, toluene soluble and the insolubles were dried until constant weights were
142 obtained by exposing them to a slight flow of Nitrogen. The jars weight changes were recorded
143 accordingly. It should be noted that the insoluble fraction might contain inorganics and coke, in principle,
144 the only organic compound insoluble in toluene [4].

145 The free trapped fluid foulants prepared in the form of powder were analysed by SEM-EDX, XRD
146 and combustion analysis (CHN). For this study, a JEOL JSM-6010LA model SEM equipped with an
147 Oxford INCA EDXS system was employed at an accelerating voltage of 20kV, and a working distance
148 ranging from 15 to 20mm to detect SE and X-rays emissions. Samples were nonconductive dried powder

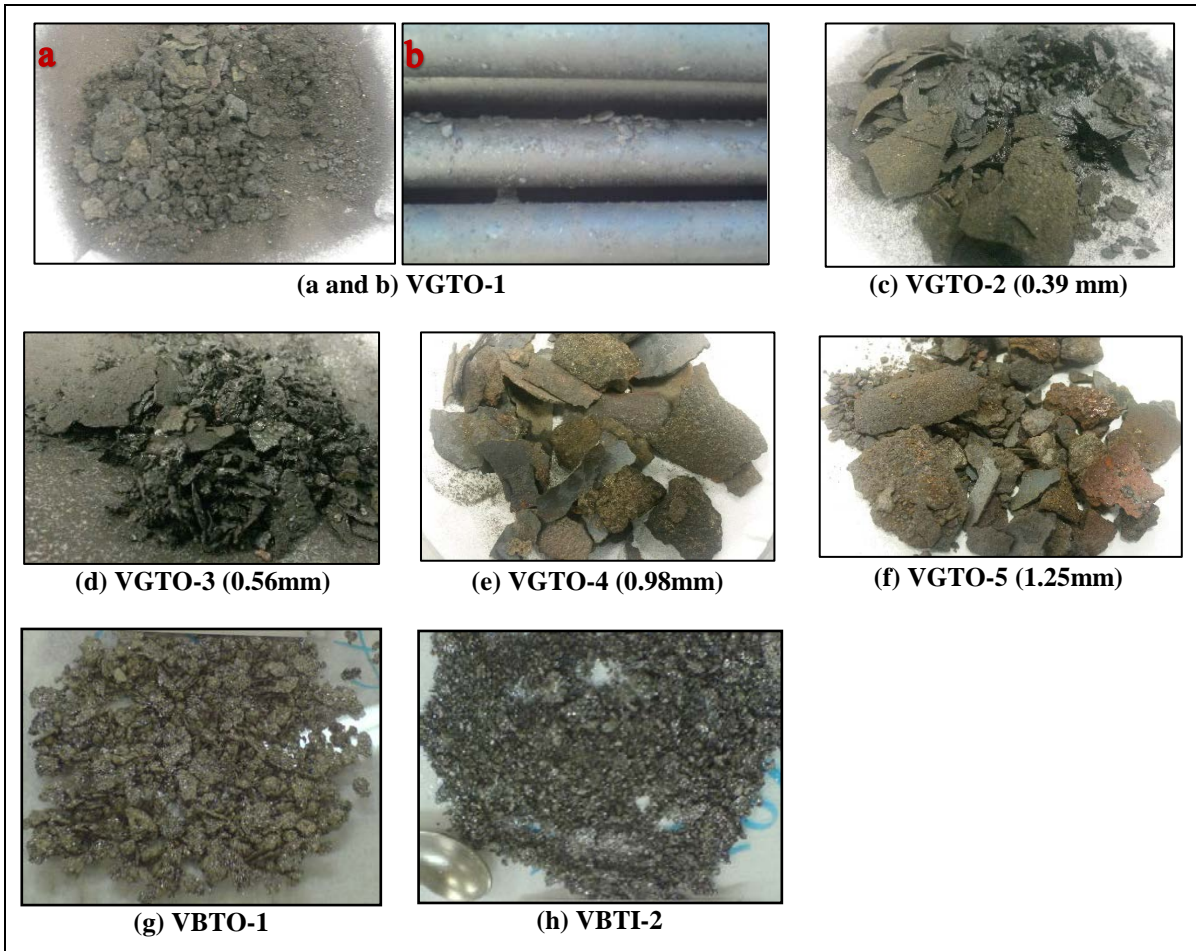
149 with particle size larger than 1 μm , hence the analysis were carried out at high vacuum. The samples were
150 mounted on a carbon tape which was stuck on a specimen stub. Excess particles were blown off with
151 compressed air to remove piled particles, and coated with an ultrathin layer of gold. As for XRD analysis,
152 foulant diffraction patterns were determined by an X'Pert Pro diffractometer (from PAN analytical) while
153 mineral compositions were identified using PANalytical X'Pert HighScore Plus. To determine the weight
154 percentage of C, H and N contents, 2mg of the prepared samples was provided to a CHN analyser (Medac
155 Ltd., UK) for the combustion analysis.

156 **3. Results and Discussion**

157 3.1. Morphology and physical characteristics

158 Fig. 1 illustrates the general appearance of samples in images taken with a digital camera. The fouled
159 layers deposited by VGO covered peripherally all-over the exchangers' tubes length, except for VGTO-
160 1. The latter sample was collected from the tubes of the coolest exchanger (E1A). Its fouling deposit
161 presented significantly less volume and exhibited particulates in nature, as shown in Fig. 1, VGTO-1(b).
162 The foulant thickness, indicated beneath the corresponding images, became thinner as the operating
163 temperatures decreased. Interestingly, samples deposited in the exchangers with the same mechanical
164 design specifications (i.e., E3A and E3B, E2A and E2B, see Table 1) had similar appearance. However,
165 those formed at the hotter shells of A (i.e., VGTO-5 and VGTO-3), were thicker (by 28% and 44%,
166 respectively) and more brittle when collected. VB foulants deposited both inside (VBTI-1) and outside
167 (VBTO-2) the exchangers' tubes had a metallic lustre appearance, with the former being like black
168 particulates and the latter exhibiting a brighter flaky look.

169

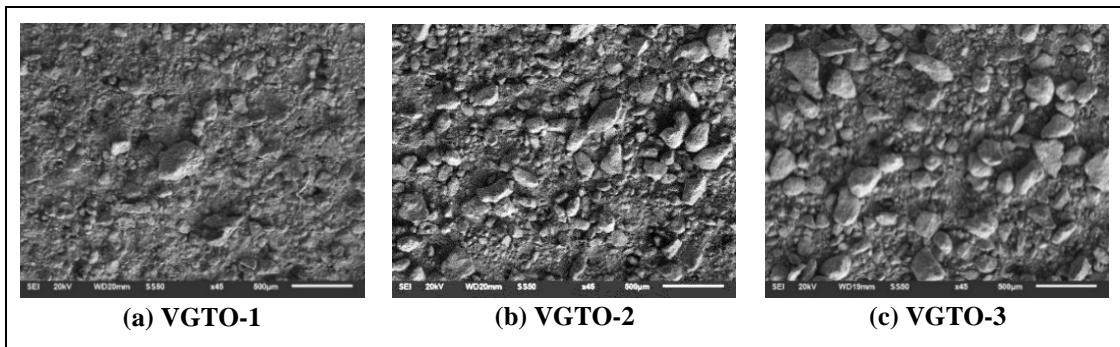


170 **Figure 1-General appearance of raw foulant samples (foulant layer thickness given in mm where possible)**

171

172 The microscopic topography of foulant particles was examined by SEM images taken at 500 μ m
 173 resolution and is presented in Fig. 2. Irregularly shaped particles in various quantity and sizes are observed,
 174 ranging from mostly fine aggregates to large agglomerated ones. Particles in VB foulant samples appeared
 175 more like polyhedral clusters with sharp edges.

176



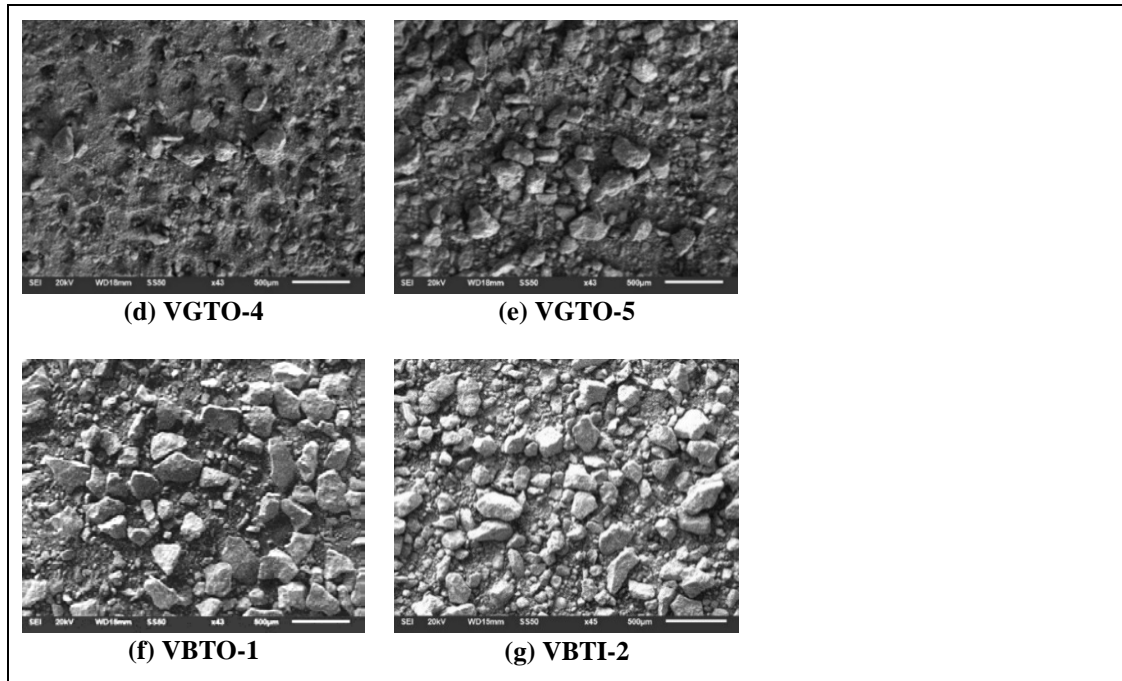


Figure 2- SEM images of foulant samples taken at a 500µm resolution

177

178

179 The number of large agglomerated particles was quantified using a Digimizer software. First, the
 180 surface area of particles larger than a specific base size (here assumed 0.02 mm², as indicated in Fig. 3)
 181 was calculated. The number of particles was then counted and the results were illustrated graphically,
 182 together with an average surface areas value for all large particles in the sample (Fig.4). Apart from
 183 VGTO-1, a sample which consisted mostly of fine aggregates, the number of large particles as well as the
 184 average surface area seems to be greater for the VB foulant samples. In VGO samples, both quantities
 185 were higher for foulants deposited in the hotter exchanger shells having the same design specifications.
 186 As explained below, the deposits formed in the hotter shells were thicker and more brittle. Therefore, the
 187 results seem to indicate that these properties are related to the number of large particles.

188

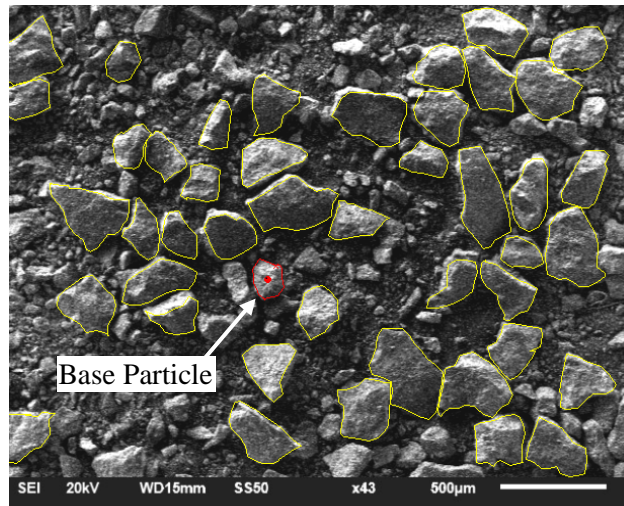


Figure 3- Large particle count in the SEM image (VBTO-2)- The base particle is indicated by the arrow

189

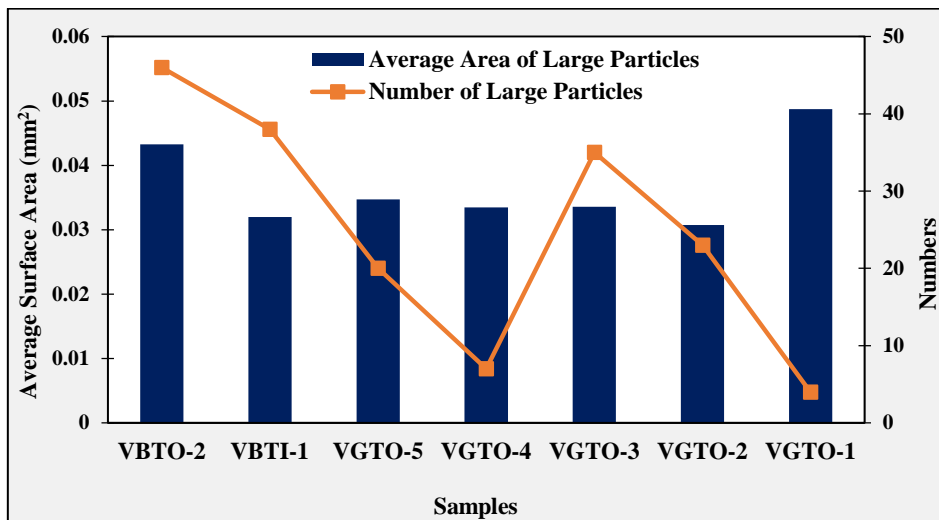


Figure 4- Number of large particles and their average surface areas in the foulant samples

190

191

192

193 3.2. Chemical characteristics

194 The three fractions obtained after solvent extraction of the raw foulant samples are detailed in Table 2
 195 in terms of wt% of maltenes, asphaltenes and insoluble parts. It is worth noting that VGO is an
 196 asphaltenes- free fraction of crude oil; very small increases in the asphaltenes jars weights observed for
 197 several samples were considered as analysis error and were therefore adjusted by adding them to the
 198 insoluble fraction. Amongst the VGO foulant samples examined (see Table 2), those deposited at higher
 199 temperatures contained less maltenes, and greater insoluble contents, similar to the VB's foulants which

200 contained nearly 3% asphaltenes. Given the high content of inorganics in all samples tested, scaling,
 201 corrosion and particulate deposition were considered the most likely dominant fouling mechanisms.

202

203 **Table 2- Fractions contents (wt%) specified with solvent extraction of raw foulant samples**

Samples	VGTO-1	VGTO-2	VGTO-3	VGTO-4	VGTO-5	VBTO-1	VBTI-2
Maltenes	24.76	19.74	18.18	17.98	15.86	14.56	7.35
Asphaltenes	---	---	---	---	---	2.47	3.21
Insoluble	75.24	80.26	81.82	82.02	84.14	82.96	89.44

204

205 Results of the EDX, CHN and XRD analysis on the free trapped fluid samples are summarised in
 206 Table 3. EDX determined the relative weight percentage of most elements in the samples except for
 207 carbon and hydrogen which were specified by combustion analysis in absolute terms. Hence, the relative
 208 EDX results were normalized in order to provide an appropriate comparable data, according to Joshi's
 209 approach, which involves setting up a mass balance between the obtained data [8]. As can be seen from
 210 Table 3, for nearly all samples taken from the VGO and VB heating fluids, the content of C, H, N, O, S
 211 and Fe was significant (higher than ~1.0wt%), and composed partly by FeS, FeO(OH) and S in crystalline
 212 forms as indicated by their peaks indexed on the XRD patterns of Fig. 5. Interestingly, peaks associated
 213 with FeS were clearly repeated in all of the patterns, while FeO(OH) peaks seem to exist only in VGTO-
 214 5, VGTO-4 and VBTI-2, with S peaks being observed just in the first two. The relatively small percentage
 215 of C indicates that the organic material in the raw deposit samples was most likely trapped, non-coked oil;
 216 therefore material soluble in heptane and washed away from samples during the preparation step.

217 It should be mentioned that Na content in the VB samples was noticeable (0.87wt% and 2.07wt%)
 218 compared to that in VGO samples (0.00-0.23wt%). However, fouling concerns caused by VB as heating
 219 fluid were insignificant compared to those of VGO and as such, the role of Na was not considered in the
 220 discussion that follows.

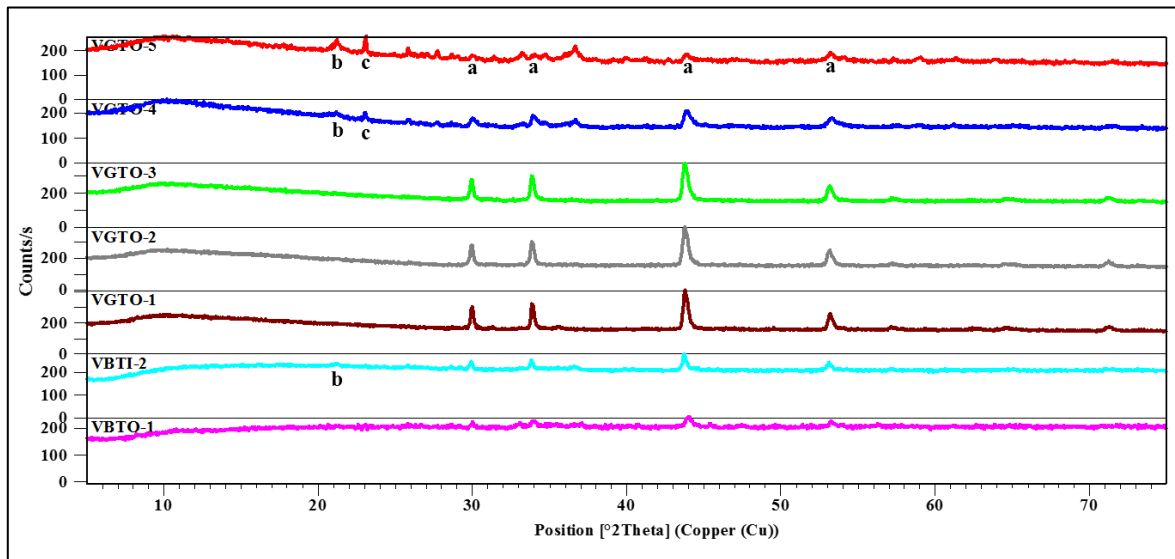
221

222

Table 3- Elements' contents (%wt) and crystalline compounds of foulant samples

Samples	VGTO-1	VGTO-2	VGTO-3	VGTO-4	VGTO-5	VBTO-1	VBTI-2
C	3.99	1.61	1.81	2.22	2.08	4.23	3.27
H	0.99	0.97	0.91	1.37	1.60	1.27	1.35
N	0.24	0.85	1.64	1.60	2.61	3.28	1.63
O	17.08	19.02	17.92	33.49	39.24	43.95	39.17
S	25.70	26.11	25.70	21.54	19.42	14.40	13.39
Fe	51.10	50.58	50.61	39.02	34.53	29.10	39.61
Na	0.00	0.01	0.23	0.00	0.00	2.07	0.87
Mg	0.00	0.13	0.14	0.11	0.00	0.10	0.10
Ca	0.25	0.25	0.28	0.25	0.23	0.21	0.12
Si	0.27	0.04	0.19	0.14	0.13	0.44	0.26
Cl	0.03	0.10	0.03	0.00	0.00	0.74	0.09
V	0.04	0.02	0.08	0.26	0.14	0.14	0.13
Ni	0.32	0.31	0.45	0.01	0.00	0.07	0.01
Crystalline Compounds	FeS	FeS	FeS	FeS FeO(OH) S	FeO(OH) FeS S	FeS	FeS FeO(OH)

223



224

225

Figure 5- Indexed XRD patterns of foulant samples (a, b and c stands respectively, for FeS, FeO(OH) and S)

226

227

228

229

230 3.3. Fouling Mechanism Determination

231 The evidence relating to tube materials, operating temperatures of exchangers, foulant layers thickness,
232 insoluble fraction, elements and compounds identified (see Fig. 1 and Tables 1-3) point to the followings
233 remarks:

- 234 a. More than 75wt% of each free trapped fluid sample were inorganic matter, mostly (>50%) in
235 the form of Fe and S elements, which were deposited at temperatures lower than 300°C. Based
236 on XRD evidence, Iron sulphide (FeS) existed in all of them.
- 237 b. Foulant layers were thicker in the first two VGO samples deposited at higher operating
238 temperatures on Cr-Mo alloy tubes (VGTO-5 and 4) compared to those formed on the outer
239 surfaces of CS tubes at lower operating temperatures (VGTO-3 and 2), while the former had
240 less Fe and S content.
- 241 c. FeO(OH) existed only in samples deposited at higher temperatures in both VG or VB foulants
242 on tube surfaces made of Cr-Mo alloy.

243 These observations are in line with the findings of several laboratory studies made on petroleum
244 corrosion as summarized in Table 4. At temperatures below 350°C, corrosion is the predominant
245 mechanism, as opposed to coke fouling [14]. This agrees with the identification of more than 50wt% Fe
246 plus S elements in the foulant samples studied here, which were deposited below 300°C. Hence,
247 Naphthenic acids (NAP, RCOOH) and sulphur compounds should be investigated as the main causing
248 species. Also, as far as foulant thickness and corrosion rate of the surfaces made by Cr steel and CS alloy
249 are concerned, similar observations to [15] [16] were made in this study, indicating that less corrosion and
250 more fouling may be expected with Cr alloy surfaces in comparable conditions. Additionally, the
251 identification of Fe and O compositions in the foulant samples deposited on Cr steel alloy at higher
252 temperatures reported in this work, as well as those investigated in [17] [18] [19] (see Table 4), indicate
253 that deposition temperature also plays an important role on the corrosion reaction types involved and their
254 resulting products. When faced with oxygen detection in examining corrosion products, its presence was

255 previously dismissed in several laboratory studies as due to either exposure to air contamination or
 256 experimental errors [18].

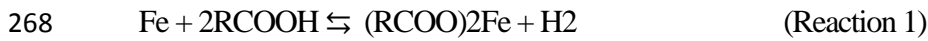
257

258 Table 4- A summary of results for the latest laboratory case studies on petroleum corrosion

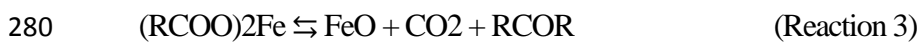
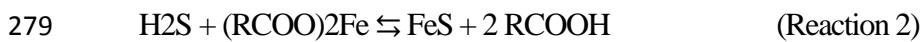
No	Subject (Process fluid)	i) Observation / ii) Comment	Ref
1	Iron sulphide and coke fouling (sour oil)	i) Prevalence of corrosion over coke fouling at temp <350°C. ii) NAP and S compounds are main species, causing petroleum corrosion leading to FeS particulates or film fouling.	[14]
2	Sulphide promoted chronic fouling on heat transfer surfaces made of different metallurgies at T _{bulk} =290°C, T _{surface} =490°C (two crude oil blends)	i) Thicker foulant (~ 2×) on wire surface made of 9Cr-Mo steel compared to CS with the most cross section reduction. ii) 'self-cleaning' behaviour of CS, i.e. sulphide forms on surface, but continuously delaminates during test, leading to reduced sulphide/coke build-up rates and its cross section.	[15]
3	Competitive corrosion mechanisms of NAP and sulphur compounds (crude oil)	i) Corrosion layers formed on 5Cr steel surfaces were more protective against NAP attacks than those formed on CS surfaces.	[16]
4	FeS protectiveness, NAP challenge attacks on FeS scale (VGO)	i) Presence of an iron oxide layer on the least corroded metal surface. ii) A probable oxygen source of the oxide layer is NAP acids in the crude fraction, thermally decomposed during the test.	[17]
5 6	Analysis of corrosion scales formed on CS and 5Cr steel surfaces in hydrocarbons containing different values of NAP and S compounds (crude oil)	i) The oxide layer (magnetite, Fe ₃ O ₄) protected surface against NAP attacks, and not the FeS layer. ii) - Magnetite originated from NAP corrosion, iron naphthenates decomposition and disproportionation of FeO. - layers formed on 5Cr steel surfaces were more protective than those on CS surfaces, perhaps Cr acts as catalyst in forming magnetite and enhancing protectiveness. - No oxide scale, even in the presence of NAP, following similar experiments with first phase of scale formation at low temperature (232°C), could prove the importance of higher temperatures in overcoming NAP corrosion compared to sulphidation.	[18] [19]

259

260 Having reviewed the above evidence, a novel corrosion mechanism is proposed here to describe the
 261 fouling process experienced in the refinery exchangers where our foulant samples were collected. The
 262 presence of Cr in the alloys could enhance surface resistance against sulphur compounds attacks.
 263 However, at high temperatures (270–280 °C), the Cr alloy surface might not resist against NAP attacks,
 264 leading to Reaction 1 and production of oil-soluble iron naphthenates, (RCOO)₂Fe, which have a size
 265 twice that of naphthenic acid. Hence, the larger (RCOO)₂Fe would diffuse back to the bulk fluid more
 266 slowly than the NAP (responsible for acid attacks) diffuse from the bulk fluid to the tube surface, thereby,
 267 providing a diffusion barrier to the steel surface.



269 On the other hand, as a result of an iron naphthenates possible reaction with H₂S (Reaction 2), FeS
270 particulates may deposit on the barrier and, given time at this high temperature, the naphthenates
271 decompose to FeO (Reaction 3). The latter is thermodynamically unstable, and hence disproportionates
272 further to magnetite (Fe₃O₄) (Reaction 4). These seemingly stagnant compounds on the exchanger tube
273 surfaces where heavy oil fractions such as VGO or VB are flowing, may transform into thick foulant
274 layers. This would therefore justify the presence of thicker foulant layers and less corrosion observed at
275 the hotter exchangers whose tube surfaces were made from Cr steel alloys, i.e. E3AB and E5 (see Table
276 1). Temperature in the downstream exchangers (E2AB, E1A and E4) was not high enough for Reaction
277 1 to take place, but as their surfaces were made from CS, sulphidation (Reaction 5) might have occurred,
278 leading to the production of a FeS layer.



283 Although the produced FeS layer could protect the metal surface against subsequent H₂S attacks, it
284 may be assumed that in this temperature range NAP reacts backward with FeS (Reaction 2) to stabilize
285 the equilibrium by regenerating H₂S. FeS dissolution or delamination of primarily formed scales would
286 encourage further sulphidation leading to more corrosion and less fouling, as experienced in the
287 downstream exchangers named above.

288 As regards the presence of FeO(OH) in foulant samples from E3AB and E5, it is worth noting that no
289 Fe₃O₄ (produced by Reaction 4) was identified in our XRD results. Fe₃O₄ might somehow have reacted
290 with water and turned into FeO(OH) according to Reaction 6. Considering the unlikely presence of water
291 in heavy oil fractions, water circulation and steam purging, carried out as a mandatory operation before

292 dismantling the exchangers in a major shutdown, may have been responsible for such reaction and justify
293 our results.

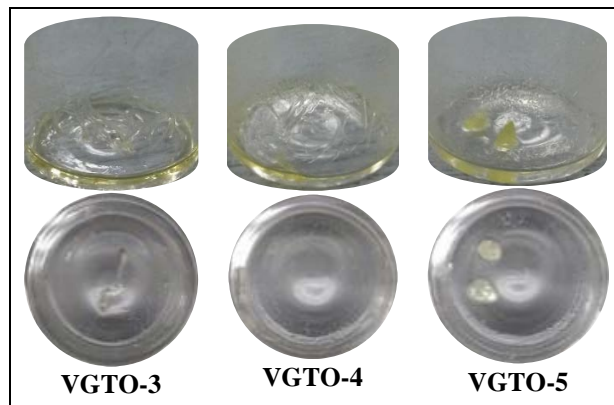


295 It should be noted that more Fe was observed in VBTI-2 sample collected from inside the Cr-Mo alloy
296 tubes of E5 compared to the VBTO-1 sample from the CS outside tube of E4. This could be explained
297 by deposition of particulates originated from upstream equipment corrosion products or Fe compounds
298 suspended in the fluid, for which it is required to examine the suspended solid particles content of VB at
299 the entrance of the corresponding exchangers. This could also be carried out for VGO to determine the
300 possible contribution of particulate deposition on forming thick fouling layers (1mm and above). It is
301 postulated that the suspended particles might be dragged along with the heavy fractions streams and
302 eventually settle in the product side of the heat exchangers. The attachment of such particles would indeed
303 be facilitated by the presence of a deposit layer formed, initially, following a local corrosion mechanism
304 as proposed above. At the high temperatures of the VGO and VB streams, the corrosion particles (e.g.
305 FeS) may act as “nucleation” points for the formation of coke, which in turn could act as a gluing agent
306 and lead to particle agglomeration [15]. From the time the particles detach at upstream equipment to the
307 time when they deposit at the heat exchanger, the dimensions and characteristics of the particles would
308 therefore evolve. This might explain the wide range of particle sizes observed in this study, as well as the
309 differences between deposits formed by each fluid (VB and VGO) and at different locations along the
310 line for each of them.

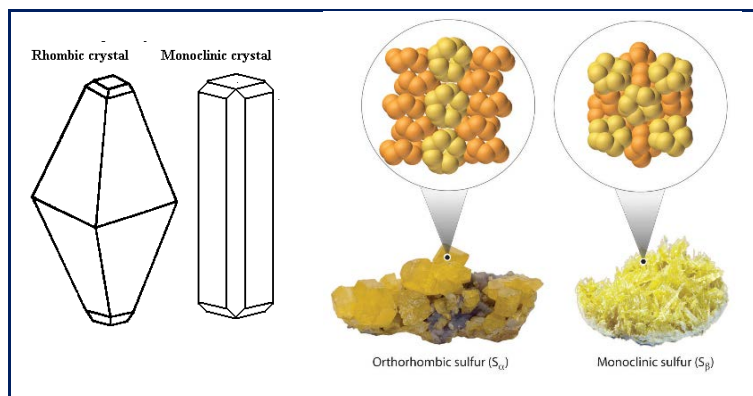
311 3.4. The existence of sulphur crystals

312 As can be seen in Figure 5, a special peak is observed in the XRD patterns of VGTO-5 and 4
313 corresponding to sulphur (indexed by letter c). During the extraction analysis, after drying the n-heptane
314 solvent by nitrogen flow, some crystals became evident in the maltenes jars of these samples as well as
315 those of VGTO-3 (Fig 6). Both sulphur allotropes illustrated in Fig. 7 [20] were seen in the VGTO-5 jar:
316 two large orthorhombic crystals (2-4mm in size) at the bottom, and a mass of monoclinic ones on the

317 peripheral surface. For VGTO-4 and VGTO-3, only monoclinic crystals in larger sizes were observed.
318 However, S crystal peaks were not identified in the XRD pattern of VGTO-3, perhaps due to smaller
319 amount of S crystals being washed away by n-heptane during sample preparation of XRD examination.
320 The tube material (CS) might also have played a role here through a sulphidation reaction.
321



322 **Figure 6- Maltenes jars of VGTO-3, 4 and 5 samples, following drying with nitrogen flow.**
323 **Sulphur crystals are clearly evident in both allotropes**
324



325 **Figure 7- Illustration of two allotropes of Sulphur [20]**
326

327 **4. Conclusions**

328 A comprehensive investigation was carried out on the morphological, physical and chemical
329 characteristics of seven foulant samples deposited below 300°C by VGO and VB as heating fluids in
330 preheaters of a constant feedstock distillation unit. Results show that more than 75wt% of all samples
331 were inorganics (indicated by insolubility in n-heptane and toluene), with 50wt% FeS. Additionally,
332 FeO(OH) was also deposited on hotter tube surfaces made from Cr steel alloy, where more fouling and

333 less corrosion were evident. Our results are consistent with several recent petroleum corrosion laboratory
334 studies. The role of temperature and tube material were reviewed and a mechanism was proposed to
335 explain the corrosion fouling progress experienced. According to this model, at the temperature range of
336 270-300°C, naphthenic acid attacks tube surfaces made from Cr steel alloy, leading to the formation of a
337 corrosion-protective foulant layer consisting of FeO(OH) as well as FeS particulates, produced by reaction
338 of H₂S and (RCOO)₂Fe (iron naphthenates). For CS-tube exchangers working at lower temperatures,
339 sulphidation creates FeS layers which delaminate by reacting with naphthenic acid, regenerating H₂S and
340 causing further corrosion. This corrosion process could also explain the formation and detachment of
341 particles in upstream equipment. After being dragged by the heavy fractions streams, and agglomerated
342 over time into different sizes and morphologies, these particles might have deposit on the product side of
343 the preheaters, leading to the observed deposit layers of 1 mm thickness and above.

344 The results not only agree with observations made in laboratory test, but also highlight the importance
345 of studying deposits formed under industrial conditions, timescales and variation of the deposition
346 process, evidenced by the deposit characteristics, along extensive heat exchanger networks. Furthermore,
347 XRD patterns indicated the existence of sulphur crystals in several of the VGO foulant samples,
348 confirmed by observation in the forms of both allotropes in their maltenes fractions.

349

350 **Acknowledgements**

351 EB and MRM gratefully acknowledge collaboration of EORC refinery. Also, the authors wish to
352 thank Dr Marcos Millan-Agorio for provision of laboratory facilities.

353

354 **References**

- 355 [1] Macchietto S, Hewitt GF, Coletti F, Crittenden BD, Dugwell DR, Galindo A, et al. Fouling in Crude Oil
356 Preheat Trains: A Systematic Solution to an Old Problem. *Heat Transf Eng* 2011;32:197–215.
- 357 [2] Coletti F, Joshi HM, Macchietto S, Hewitt GF. Introduction to Crude Oil Fouling. In: Coletti F, Hewitt
358 GF, editors. *Crude Oil Fouling Depos. Charact. Meas. Model.*, Boston: Gulf Professional Publishing;
359 2014.
- 360 [3] Crittenden BD, Kolaczowski ST, Downey IL. Fouling of crude oil preheat exchangers. *Trans IChemE,*
361 *Part A, Chem Eng Res Des* 1992;70:547–57.
- 362 [4] Brons G, Brown LD, Joshi HM, Kennedy RJ, Bruno T, Rudy TM. Method for refinery foulant deposit

- 363 characterization. US 2006/0014296A1, 2006.
- 364 [5] Bennett CA, Appleyard S, Gough M, Hohmann RP, Joshi HM, King DC, et al. Industry-Recommended
365 Procedures for Experimental Crude Oil Preheat Fouling Research. *Heat Transf Eng* 2006;27:28–35.
366 doi:10.1080/01457630600845788.
- 367 [6] Venditti S, Berruoco C, Alvarez P, Morgan TJ, Millan M, Herod AA, et al. Developing Characterisation
368 Methods for Fouling Deposited in Refinery Heat Exchangers. *Int. Conf. Heat Exch. Fouling Clean.*
369 VIII, vol. 2009, Schladming, Austria: 2009, p. 44–51.
- 370 [7] Young A, Venditti S, Berruoco C, Yang M, Waters A, Davies H, et al. Characterization of Crude Oils
371 and Their Fouling Deposits Using a Batch Stirred Cell System. *Heat Transf Eng* 2011;32:216–27.
372 doi:10.1080/01457632.2010.495603.
- 373 [8] Chew J, Joshi HM, Kazarian SG, Millan-Agorio M, Tay FH, Venditti S. Deposit Characterization and
374 Measurements. In: Coletti F, Hewitt GF, editors. *Crude Oil Fouling*. First, Elsevier Inc.; 2015, p. 95–
375 178. doi:10.1016/B978-0-12-801256-7.00004-X.
- 376 [9] Mozdianfard MR, Behranvand E. A field study of fouling in CDU preheaters at Esfahan refinery. *Appl*
377 *Therm Eng* 2013;50:908–17. doi:10.1016/j.applthermaleng.2012.08.025.
- 378 [10] Mozdianfard MR, Behranvand E. Fouling at post desalter and pre flash drum heat exchangers of CDU
379 preheat train. *Appl Therm Eng* 2015;89:783–94. doi:10.1016/j.applthermaleng.2015.06.045.
- 380 [11] Brons G, Brown LD, Joshi HM, Kennedy RJ, Bruno T, Rudy TM. Method for refinery foulant deposit
381 characterization. US 2006/0014296 A1, 2010.
- 382 [12] Puron H, Pinilla JL, Berruoco C, Fuente JAMD Ia, Millan M. Hydrocracking of Maya Vacuum Residue
383 with NiMo Catalysts Supported on Mesoporous Alumina and Silica–Alumina. *Energy and Fuels*
384 2013;27:3952–60.
- 385 [13] Puron H, Chin KK, Pinilla JL, Fidalgo B, Millan M. Kinetic analysis of vacuum residue hydrocracking
386 in early reaction stages. *Fuel* 2014;117:408–14. doi:10.1016/j.fuel.2013.09.053.
- 387 [14] Wang W, Watkinson AP. Iron Sulphide and coke fouling from sour oils: review and initial experiments.
388 In: Malayeri MR, Müller-Steinhagen H, Watkinson AP, editors. *Int. conf. heat Exch. fouling Clean.*
389 2011, vol. 2011, Crete Island, Greece: 2011, p. 23–30.
- 390 [15] Hazelton M, Stephenson T, Lepore J, Subramani V, Mitlin D. Sulfide promoted chronic fouling in a
391 refinery: A broad phenomenon spanning a range of heat transfer surfaces and oil types. *Fuel*
392 2015;160:479–89. doi:10.1016/j.fuel.2015.07.074.
- 393 [16] Bota G, Nestic S. Naphthenic Acid Challenges to Iron Sulfide Scales Generated In-Situ from Model Oils
394 on Mild Steel at High Temperature. *NACE Int. Corros. Conf. Expo*, 2013, p. 1–13.
- 395 [17] Bota GM, Farelas F, Robbins W, Nestic S. Evaluation of Scales Protective Properties in Naphthenic
396 Acid Challenges. 248th ACS Natl. Meet. Expo., 2014, p. 546.
- 397 [18] Jin P, Nestic S, Wolf HA. Analysis of corrosion scales formed on steel at high temperatures in
398 hydrocarbons containing model naphthenic acids and sulfur compounds. *Surf Interface Anal*
399 2015;47:454–65. doi:10.1002/sia.5733.
- 400 [19] Jin P, Bota G, Robbins W, Nestic S. Analysis of Oxide Scales Formed in the Naphthenic Acid Corrosion
401 of Carbon Steel. *Energy & Fuels* 2016. doi:10.1021/acs.energyfuels.6b01066.
- 402 [20] Chemistry of Sulfur. UC Davis ChemWiki n.d.
403 [http://chemwiki.ucdavis.edu/Core/Inorganic_Chemistry/Descriptive_Chemistry/Elements_Organized_by](http://chemwiki.ucdavis.edu/Core/Inorganic_Chemistry/Descriptive_Chemistry/Elements_Organized_by_Block/2_p-Block_Elements/Group_16:_The_Oxygen_Family/Chemistry_of_Sulfur)
404 [Block/2_p-Block_Elements/Group_16:_The_Oxygen_Family/Chemistry_of_Sulfur](http://chemwiki.ucdavis.edu/Core/Inorganic_Chemistry/Descriptive_Chemistry/Elements_Organized_by_Block/2_p-Block_Elements/Group_16:_The_Oxygen_Family/Chemistry_of_Sulfur).